



ELSEVIER

Spectrochimica Acta Part B 55 (2000) 1759–1769

SPECTROCHIMICA
ACTA
PART B

www.elsevier.nl/locate/sab

Optimization of lead metastable production in a low pressure argon discharge

C. Vadla^{a,*}, M. Movre^a, R. Beuc^a, J. Franzke^b, H.-D. Wizemann^c,
K. Niemax^b

^a*Institute of Physics, Bijenicka 46, HR-10000 Zagreb, Croatia*

^b*Institute of Spectrochemistry and Applied Spectroscopy (ISAS), Bunsen-Kirchhoff-Strasse 11, D-44139 Dortmund, Germany*

^c*Institute of Physics, University of Hohenheim, Garbenstrasse 30, D-70599 Stuttgart, Germany*

Received 16 June 2000; accepted 5 August 2000

Abstract

The spatial distribution of $6p^2\ ^3P_1$ and $6p^2\ ^3P_2$ lead metastable atoms in a radially symmetric low pressure argon discharge has been investigated by absorption measurements. The number density of lead as well as the argon pressure were varied independently. The measurements performed to find optimum conditions for metastable production in the discharge also revealed the diffusion and the collisional depopulation of the metastable species in argon. © 2000 Elsevier Science B.V. All rights reserved.

Keywords: dc Discharge; Lead; Metastable atoms; Diffusion; Collisional depopulation

1. Introduction

Recently, we have demonstrated the application of the isotope dilution technique in diode laser atomic absorption spectroscopy (DLAAS) in a graphite tube atomizer with integrated dc discharge operated in argon at low pressure [1]. It was shown that accurate and precise measure-

ments of Pb are possible independent on physical and chemical matrix effects which can be very severe if, in particular, metastable atoms are subject to measurements. Unfortunately, due to the low population density of the metastables, the detection limit of Pb was unsatisfactorily high for DLAAS.

The aim of the present paper was to better understand the physical processes in dc low pressure discharges in order to improve the metastable population of lead for DLAAS. Therefore, a very simple, radially-symmetric low pressure dc argon

* Corresponding author. Fax: +385-1-4680-397.

E-mail address: vadla@ifs.hr (C. Vadla).

plasma was set up in a temperature and pressure controlled lead–argon gas mixture. The simplicity and the radial symmetry are important for the measurements and theoretical modeling of the spatial distribution of the Pb metastable atoms and the evaluation of their diffusion and collisional quenching in the argon plasma.

2. Experiment

The spatial population distributions of lead atoms in the $6p^2\ ^3P_1$ and $6p^2\ ^3P_2$ metastable states were obtained by measurements of absorption depths of the 368.4 and 405.9-nm lines, belonging to the $6p^2\ ^3P_1 \rightarrow 7s\ ^3P_0^o$ and $6p^2\ ^3P_2 \rightarrow 7s\ ^3P_1^o$ transitions, respectively. The spatial distributions of the higher excited atoms were determined by emission intensity measurements of the optically thin 405.9-nm line. The measurements were performed in a stainless-steel hot-pipe oven (inner diameter: 30 mm; length: 400 mm) with quartz windows at the ends (see Fig. 1) and filled with argon as a buffer gas. The Pb vapor was generated by resistive heating of the central part of the oven containing a high-purity Pb sample. In the middle of the lead vapor column (length: approx. 40 mm), a dc discharge was operated between two electrodes made of stainless-steel rods (diameter: 2 mm). The discharge was driven by a current-sink power supply (voltage: 700 V; maximum current: 50 mA). Insets (a) and (b) in Fig. 1 show the two different electrode arrangements which were used in this experiment. In both cases, the distance between the electrodes was 8 mm. The vapor temperature was determined from the Doppler width of the Pb 405.9-nm line. The measurement of the Doppler width was performed by diode-laser absorption in the same manner as reported in a previous work [2]. Therefore, this part of the experiment will be not described here. The lead number density was determined from the vapor pressure curve given in [3]. The measurements were performed at several argon pressures in the range between 15 and 90 mbar.

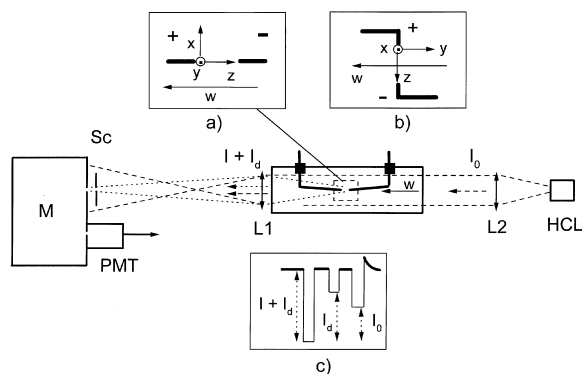


Fig. 1. Experimental arrangement. HCL, hollow cathode lamp; L, lenses; w, optical axis; Sc, screen with a pinhole; M, monochromator; PMT, photomultiplier. Insets (a) and (b). Axial and perpendicular electrode arrangement, respectively. Inset (c). Typical signals: total intensity $I + I_d$, intensity I_d measured by blocking the hollow cathode beam before passing the oven, and intensity I_0 measured by turning off the discharge.

The discharge zone was imaged by the lens L1 (focal length: 200 mm) in a 1:2 ratio onto the entrance slit of a 0.5-m Jarell–Ash monochromator supplied by a RCA 1P28 multiplier. The monochromator was used as a band-pass filter and tuned to the wavelength of either the Pb 405.9 or Pb 368.4-nm line. The absorption measurements were performed with collimated light from a Pb hollow cathode lamp. A pinhole (diameter: 0.5 mm) was placed at distance of 10 mm in the front of the monochromator entrance slit (width: 0.2 mm). In this way, the measured light absorption and emission was related to the volume having a form of a long and thin stick parallel to the optical axis. The observation volume was scanned by shifting the imaging lens in the plane perpendicular to the optical axis with a resolution of approximately $0.25 \times 0.25\text{ mm}^2$. The transmitted hollow-cathode light was discriminated from the discharge emission intensity I_d by alternative blocking of the light beam before and after passing the oven, and by additional turning off the discharge current for a short time. Typical signals are given in Fig. 1, inset (c). Using the measured incident intensity I_0 and transmitted intensity I of the hollow cathode lamp at the wavelength of the

particular spectral line, we obtained position-dependent optical depths K as:

$$K = -\ln\left[\frac{I}{I_0}\right]. \quad (1)$$

The frequency- and position-dependent absorption coefficient of the lines can be expressed as $k(\nu) = q N P(\nu)$, where q is the factor comprising characteristic parameters of the relevant transition, N is the number density in the corresponding metastable state, and $P(\nu)$ is the normalized line profile. The profiles of the considered lines are compositions of several hyperfine and isotope components. As shown in [2], the profiles of particular components in absorbing volume are shifted (argon pressure shift) convolutions of the Gaussian (Doppler broadening) and Lorentzian function (argon pressure broadening) at the present experimental conditions. On the other hand, the incident hollow cathode light was characterized by optically thin 368.4 and 405.9-nm lines. The pressure shift of the hollow cathode lines is negligible and they are essentially Doppler broadened (temperature: approx. 350 K). The monochromator (spectral resolution: 0.03 nm) integrates the measured line intensity over the frequency scale and the measured optical depth can be expressed as:

$$K = -\ln\left[\frac{\int_{\nu} P_0(\nu) \exp\left(-\int_{\xi} k(\vec{r}, \nu) d\xi\right) d\nu}{\int_{\nu} P_0(\nu) d\nu}\right] \quad (2)$$

where $P_0(\nu)$ is the line profile of the incident lamp light, and ξ denotes the observation axis. Under typical conditions, the measured optical depth at 405.9 nm was approximately 30 times smaller than at the 368.4-nm line. For this reason, the experiment was focused on the 368.4-nm line, i.e. on the density populations in the lower metastable state $6p^2\ ^3P_1$. The population density of the higher metastable $6p^2\ ^3P_2$ state can be calculated with the experimental temperature (principle of detailed balancing). This is possible since, in a recent experiment [2] performed by

laser absorption under almost the same experimental conditions, it was found that the measured density ratio of $6p^2\ ^3P_1$ and $6p^2\ ^3P_2$ lead atoms was constant outside of the discharge and the value agreed with the equilibrium value calculated for the experimental temperature.

In order to obtain a relation between the number density $N_1(\vec{r})$ of the $6p^2\ ^3P_1$ metastables and the measured values for optical depth $K_1(r)$ at 368.4 nm, we calculated the integrals in Eq. (2) using the argon pressure broadening- and shift-parameters of [3]. The value for the transition probability $A = 1.7 \times 10^8\ \text{s}^{-1}$ was taken from Penkin and Slavenas [4]. In our model, $P_0(\nu)$ is represented by a sum of non-shifted Doppler-broadened components of the 368.4-nm line at $T = 350\ \text{K}$, while $P(\nu)$ is given by convolutions of Doppler and Lorentzian profiles at the experimental temperature $T = 1000\ \text{K}$. The calculations yielded that there is a linear relation (accuracy: $\pm 2\%$) between $K_1(r)$ and the value for $N(\vec{r})$ integrated over axis of observation for $K_1 < 1$ and $p_{\text{Ar}} < 100\ \text{mbar}$:

$$\int_{\xi} N_1(\vec{r}) d\xi = (1.15 + 0.0043 p_{\text{Ar}}) \times 10^{12} K_1, \quad (3)$$

where p_{Ar} is the argon pressure in mbar and the integral over the observation axis ξ is given in cm^{-2} . In this way, the linear dependence of the measured optical depth and metastable number density integral was established. In general, the optical depth K_1 is represented with a polynomial in terms of number density integrals along the observation axis, where, at present conditions, the second term becomes important for $K_1 > 1.5$ and $p_{\text{Ar}} > 100\ \text{mbar}$.

3. Measurements

The population of excited atomic states in a low-energy discharge is mainly governed by electron impact, the radiative recombination of ions and the cascade relaxation of higher bound states. The last two processes are the most probable mechanisms for population of the metastable

state. On the other hand, the main losses of metastable states are due to quenching by collisions with charged and neutral particles, and to diffusion out of the discharge volume. It was found that, for the given experimental arrangement (distances between the electrodes, inner diameter of the metal oven), a maximum portion of the lead atoms being transferred to the metastable states (approx. 30%) can be achieved if the discharge current is 30 mA, argon pressure $p_{\text{Ar}} = 40$ mbar, and the oven temperature $T = 880$ K, which corresponds to the lead number density $N_0 = 1 \times 10^{13} \text{ cm}^{-3}$. In principle higher metastable number densities could be produced either by a higher discharge current or lead number density. Unfortunately, in both cases, the discharge becomes unstable due to the higher metastable density and significant increase of conductivity of the gas layer between the electrodes and the metal wall of the oven.

In the first part of the experiment performed under the mentioned optimum conditions the discharge axis (labeled with z) was oriented perpendicular to the optical axis w . As displayed in Fig. 1, inset (b), the observation axis was labeled with y . Fig. 2 shows the measured relative intensities $I^*(x,z)$ of the optically thin 405.9-nm line while Fig. 3 shows the optical depths $K_1(x,z)$ at 368.4 nm.

The $I^*(x,z)$ data represent the distribution of the short-lived excited $7s \ ^3P_1^o$ atoms. The intensities of other short-lived lead atoms exhibited the same distribution. The intensity data represent the shape of the discharge, i.e. the volume in which metastable atoms are produced. The highest concentrations of short-lived atoms are near to both electrodes, as can be seen in Fig. 2. The entire part of the cathode exposed to the metal vapor was covered with the discharge and strongly heated. The emission intensity drops drastically between the electrodes, which indicates the absence of the positive column. The operating discharge mode can be classified as the abnormal glow discharge.

The $K_1(x,z)$ distribution reflects the spatial distribution of the metastable $\text{Pb } 6p^2 \ ^3P_1$ atoms. Due to diffusion, it is much broader than the $I^*(x,z)$ distribution. One can see that the anode

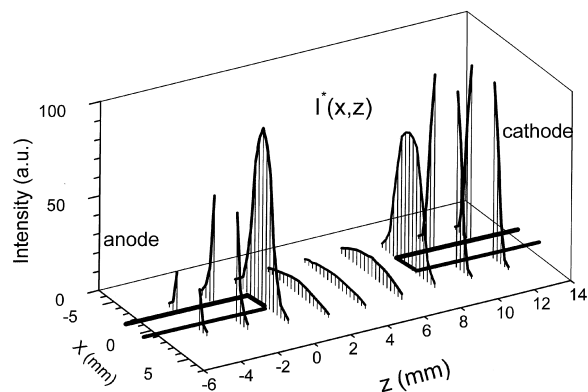


Fig. 2. Intensity distribution $I^*(x,z)$ of the optically thin Pb 405.9-nm line measured at discharge current: 30 mA, $p_{\text{Ar}} = 40$ mbar, $T = 880$ K, $N_0 = 1 \times 10^{13} \text{ cm}^{-3}$. The measurement was performed using the perpendicular electrode configuration. The distribution is related to the distribution of lead atoms in short-lived high excited states which act as sources for the population of the metastable levels.

region is more efficient for production of metastables than the cathode region. This unequal metastable production can be explained by the presence of a stronger mechanism for the metastable deactivation near the cathode. A simi-

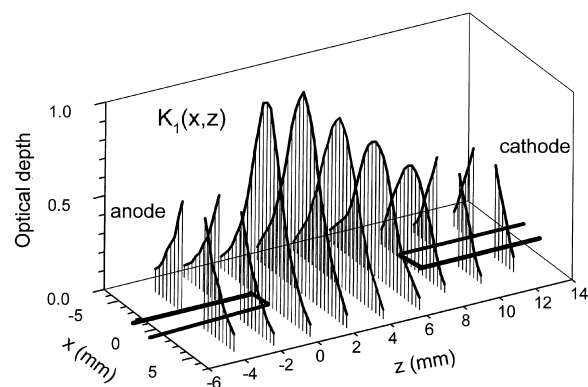


Fig. 3. Spatial distribution of the optical depth $K_1(x,z)$ at the wavelength of the Pb 368.4-nm line measured under the same conditions as in Fig. 2. The $K_1(x,z)$ is related to the spatial distribution of the lead atoms excited to the metastable $\text{Pb } 6p^2 \ ^3P_1$ state. Under the present conditions, an optimum for production of the metastable atoms was achieved. The maximum of the $K_1(x,z)$ distribution corresponds to the portion of approximately 30% of lead atoms being transferred to the metastable $6p^2 \ ^3P_1$ state.

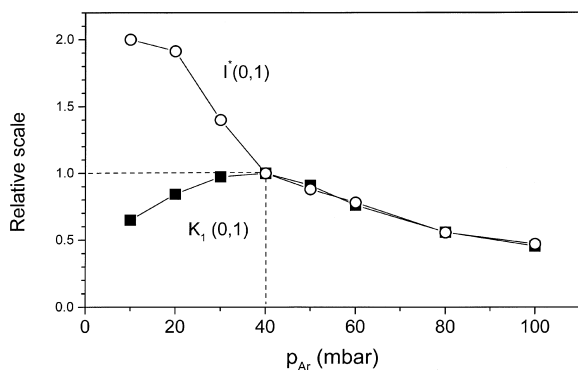


Fig. 4. Intensities $I^*(x,z)$ of the 405.9-nm line and optical depths $K_1(x,z)$ at 368.4 nm, measured in dependence on argon pressure. The other parameters (vapor temperature, discharge current, electrode configuration) are the same as in Figs. 2 and 3. The $I^*(x,z)$ and $K_1(x,z)$ were measured near the anode ($x=0$, $z=1$ mm) and both normalized to unity at $p_{Ar}=40$ mbar, where $K_1(x,z)$ reaches its maximum.

lar effect was observed in the case of metastable argon atoms in a glow discharge [5].

Fig. 4 illustrates the argon pressure dependence of the optical depth $K_1(0,1)$ and the intensity $I^*(0,1)$, both measured near the anode peak at positions $x=0$ and $z=1$ mm. The measured quantities are given in a relative scale. They are both normalized to unity at $p_{Ar}=40$ mbar where the optical depth reaches its maximum. In contrast to that, $I^*(0,1)$, representing the metastable source, exhibits its largest value at lower pressure (approx. 10 mbar). The decrease of the optical depth at low argon pressures is due to the diffusion of the metastables out of the discharge volume and their de-excitation at the walls of the oven.

The measured optical depths were radially symmetric with respect to the discharge axis, and according to Eq. (3), the number density $N_1(\rho, z)$ of the metastable Pb $6p^2\ ^3P_1$ atoms at a distance ρ from the discharge axis can be obtained from the $K_1(x,z)$ distributions by Abel inversion. Diagrams in Fig. 5 show the calculated metastable density distribution $N_1(\rho, 1)$ near the anode at position $z=1$ for various argon pressures. The temperature at the discharge axis is supposed to be higher than in the surrounding atmosphere. Therefore, the lead neutral number density is

slightly lower than outside the discharge ($N_0 = 1 \times 10^{13} \text{ cm}^{-3}$). It means that the maximum of the N_1/N_0 ratio is higher than 0.3 in the middle of the discharge. Unfortunately, we were not able to determine the gas temperature at the discharge axis. When the laser probe beam intercepts the discharge axis, the measured line absorption at the probe wavelength yields an average profile comprising the contributions outside and inside the discharge. Taking into account the shape of the metastable distributions, one can conclude that the main contribution to the measured absorption profile originates from the atoms outside the discharge. Within the error bar of the measured Doppler widths (corresponding to ± 40 K uncertainty in temperature), there was no detectable difference between the measurements performed outside the discharge and those performed with the laser probe beam intercepting the discharge axis. In addition, no temperature gradient was detected while scanning the probe laser beam across the whole volume containing the metastable atoms. This temperature isotropy outside the discharge is consistent with the findings in our previous measurement [2].

In the described experiment, the shape of the zone where metastable atoms are produced is rather complicated. We found that the simpler, and, for modeling, more convenient, form of the discharge zone can be obtained in a low-current mode (between 1 and 2 mA), which corresponds

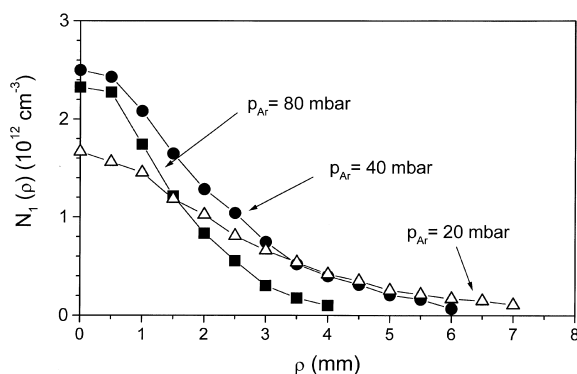


Fig. 5. Number density $N_1(\rho)$ of the metastable Pb $6p^2\ ^3P_1$ atoms near the anode ($z=1$ mm) at optimum conditions (as in Figs. 2 and 3) for metastable production at three different Ar pressures.

to the normal glow discharge. In this case, to obtain the measurable absorption related to the lead metastables, one should significantly increase the lead number density. This second part of the experiment was performed with operating current of 2 mA at a lead density of $N_0 = 5 \times 10^{14} \text{ cm}^{-3}$ ($T = 1070 \text{ K}$). The absolute values of the metastable number densities in the first and the second measurement were nearly the same. However, the relative portion of the metastable atoms in the latter is much lower than in the former case.

The intensities $I^*(x,z)$ and the optical depths $K_1(x,z)$ were measured in the same way as in the first part of the experiment [see Fig. 1, inset (b)]. The obtained distribution $I^*(x,z)$ measured at $p_{\text{Ar}} = 40 \text{ mbar}$ is given in Fig. 6. In contrast to the measurements at 30 mA, the atoms excited to the short-lived $7s \ ^3P_1^o$ state are now localized around the discharge axis within a cylinder with the radius $r_0 \approx 1 \text{ mm}$, which should be attributed to the positive column of the discharge. The corresponding optical depth $K_1(x,z)$ is shown in Fig. 7. The distribution of the $K_1(x,z)$ along z -axis has a maximum in the middle of the discharge. At this maximum, only approximately 0.5% of the lead atoms were in the $6p^2 \ ^3P_1$ metastable state at the chosen low current conditions.

Data shown in Fig. 8 illustrate the behavior of

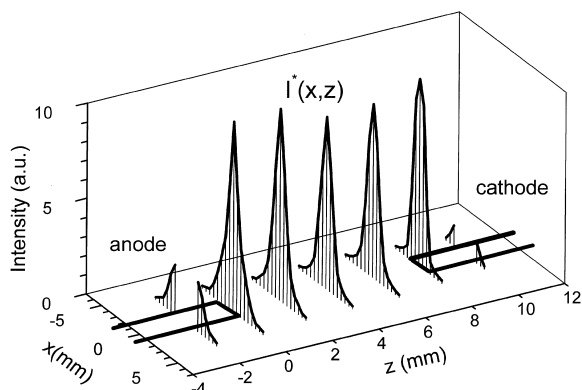


Fig. 6. Intensity distribution $I^*(x,z)$ of the optically thin Pb 405.9-nm line measured in a low current (2 mA) discharge mode. The argon pressure was 40 mbar and the lead number density $N_{\text{Pb}} = 5 \times 10^{14} \text{ cm}^{-3}$. The electrode arrangement was perpendicular.

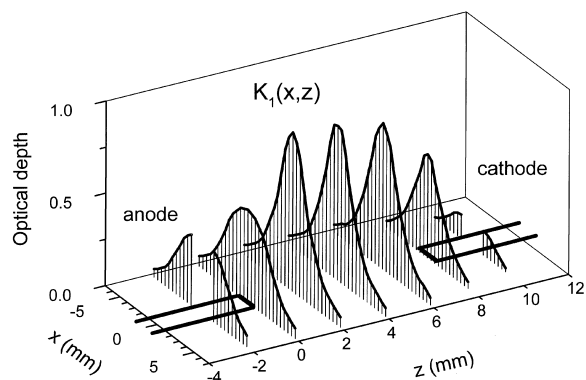


Fig. 7. Spatial distribution of the optical depth $K_1(x,z)$ at the wavelength of the Pb 368.4-nm line measured under same experimental conditions as $I^*(x,z)$ displayed in Fig. 6. In contrast to the high current discharge mode (see Fig. 3), the maximum of the K_1 displayed corresponds only to 0.5% of the lead atoms in the metastable $6p^2 \ ^3P_1$ state.

$I^*(x,z)$ and $K_1(x,z)$ distributions in dependence on argon pressure measured in the low discharge current mode. The distributions were measured in the middle of the discharge ($z = 4 \text{ mm}$) and normalized to unity at discharge axis ($x = 0$). Variations in the argon pressure produce clearly different diffusion distributions of the metastable atoms, while the distributions of the higher-excited atoms in short-lived states remain practically unchanged. The metastable distributions were also measured at constant argon pressure

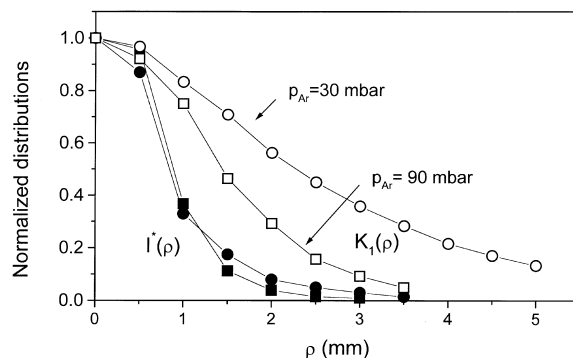


Fig. 8. Normalized intensities $I^*(\rho)$ (full symbols) and optical depths $K_1(\rho)$ (open symbols) measured at 30 (circles) and 90 mbar (squares) argon pressures in dependence on the radius ρ . The distributions were measured in the middle ($z = 1$) of the discharge operating in the low current mode and the perpendicular electrode arrangement.

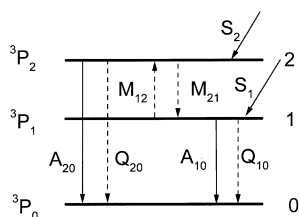


Fig. 9. Partial term diagram of lead (not in scale) including the lowest-lying states and relevant rates for population and depopulation of the Pb $6p^2\ {}^3P_j$ metastables in a electric discharge.

(40 mbar) for different lead number densities in the range between 1×10^{13} and 5×10^{14} cm^{-3} . The values for K_1 were directly proportional to the lead ground state density but these variations produced no measurable change of the distribution shape.

At low argon pressures (below 30 mbar), the diffusion of the metastables was very strong, and the cell walls, the electrodes, as well as the ends of the vapor column disturbed the metastable distributions due to recombination of the metastables.

The boundary conditions of the perpendicular electrode arrangement [Fig. 1, inset (b)] are rather complicated for theoretical modeling. Therefore, we performed the third part of the experiment under the same low current conditions as in the second part, but using the axial electrode arrangement [see Fig. 1, inset (a)], which is more appropriate for theoretical modeling. In this configuration, the discharge axis was parallel with the oven axis, i.e. with the optical axis w . These results, together with the theoretical calculations for the axial case, are given in Section 5.

4. Modeling

Fig. 9 shows the partial term diagram of lead (not in scale), including the rates relevant for the population and depopulation of lead metastables in an electric discharge. The ground state $6p^2\ {}^3P_0$ and the metastable $6p^2\ {}^3P_1$ and $6p^2\ {}^3P_2$ states are denoted with indices 0, 1 and 2, respectively. The de-excitation of the higher-lying states is the main source for metastable production represented with

source rates labeled as S_i . The depopulation of the long-lived metastables occurs mainly due to collisional mixing with the other states by charged and neutral perturbers. Regarding the energy differences between the metastable states and the other states of lead, the most probable contributions to these outgoing rates are quenching to the ground state and mutual collisional mixing, symbolized by rates Q_{i0} and M_{ij} , respectively. Radiative depopulation rates of the metastable states are labeled with A_{i0} . The lead metastable states are characterized by very small radiative relaxation rates of the order of $1\ \text{s}^{-1}$ [6]. The quenching rates Q depend on the experimental conditions and are usually represented in the form $Q = k_i N_p$, where k_i is the temperature dependent rate coefficient and N_p is the number density of the collision partner. Therefore, the effective lifetimes $\tau_i = 1/(A_{i0} + Q_{i0})$ are strongly affected by collision processes in the particular medium, which causes significant losses of the number density of metastable atoms. For instance, as reported in [7], typical effective lifetimes of the Pb $6p^2\ {}^3P_{1,2}$ metastables in air/acetylene flames at atmospheric pressure are shorter than $1\ \mu\text{s}$. Additionally, the diffusion out of the excitation zone plays an important role in establishing the metastable population balance. The loss of metastables due to diffusion depends on physical conditions and experimental geometry. Concerning a long cylindrical volume with radius r_0 where the metastable atoms are generated, the diffusion losses can be estimated by a rate $R_D = D/r_0^2$. The coefficient D is usually given in the form:

$$D = D_0 \left(\frac{p_0}{p} \right) \left(\frac{T}{T_0} \right)^{3/2}, \quad (4)$$

where p_0 and T_0 are pressure and temperature at normal conditions, respectively, and D_0 is the constant for the diffusion process. In the case of lead diffusion in argon [8], the corresponding constant $D_0 = 0.19\ \text{s}^{-1}\ \text{cm}^2$, and, for example, at $p_{\text{Ar}} = 10\ \text{mbar}$ and $T = 1000\ \text{K}$, the estimated rate for diffusion losses from the cylinder with $r_0 = 1\ \text{mm}$ amounts to $1.3 \times 10^4\ \text{s}^{-1}$.

Taking into account diffusion effects, a system

of steady-state rate equations for the metastable number densities $N_1(\vec{r})$ and $N_2(\vec{r})$ at position \vec{r} can be written as:

$$\frac{dN_1(\vec{r})}{dt} = -N_1(\vec{r})[R_{10} + M_{12}] + N_2(\vec{r})M_{21} + D\vec{\nabla}^2 N_1(\vec{r}) + S_1(\vec{r}) = 0 \quad (5)$$

$$\frac{dN_2(\vec{r})}{dt} = -N_2(\vec{r})[R_{20} + M_{21}] + N_1(\vec{r})M_{12} + D\vec{\nabla}^2 N_2(\vec{r}) + S_2(\vec{r}) = 0 \quad (6)$$

where the depopulation rate $R_{i0} = A_{i0} + Q_{i0}$.

The depopulation of the short-lived higher excited states is predominantly governed by the spontaneous radiative relaxation (order of magnitude: 10^7 s^{-1}), which is much faster than typical diffusion losses. Therefore, the spatial distributions of the higher excited states $N^*(\vec{r})$ follow the shape of the corresponding source functions $S^*(\vec{r})$. In absolute scale, source functions in a discharge are generally different for various excited states but, regarding their shapes, they are similar, and obviously restricted to the region comprising charged particles.

Assumptions about the complete collisional mixing of the considered metastable states simplifies the modeling at hand significantly. Complete collisional mixing occurs when mixing rates for a particular state are much larger than the other depopulation rates. In this case, the population densities $N_i(\vec{r})$ obey the Boltzmann distribution. The ratio $N_1(\vec{r})/N_2(\vec{r})$ becomes independent on position and, according to the principle of detailed balancing, $N_2(\vec{r})/N_1(\vec{r}) = M_{12}/M_{21} = (g_2/g_1)\exp(-\Delta E/kT)$, where g_1 and g_2 are the statistical weights and $\Delta E = 2831 \text{ cm}^{-1}$ is the fine-structure splitting of the considered metastable state. The strongly coupled system of Eqs. (5) and (6) may be solved in terms of population densities $N_1(\vec{r})$ and $N_2(\vec{r})$. Assuming that $M_{12} \gg R_{10}$, $M_{21} \gg R_{20}$ and introducing the population density of the metastable complex $N_m(\vec{r}) = N_1(\vec{r}) + N_2(\vec{r})$, the steady-state rate equation for

the population density $N_m(\vec{r})$ can be represented as follows:

$$\vec{\nabla}^2 N_m(\vec{r}) - \alpha N_m(\vec{r}) = [S_1(\vec{r}) + S_2(\vec{r})]/D. \quad (7)$$

Here, the parameter $\alpha = R_m/D$ and R_m is the depopulation rate of the metastable complex which is given by:

$$R_m = \frac{R_{i0} + R_{j0}(M_{ij}/M_{ji})}{1 + (M_{ij}/M_{ji})}. \quad (8)$$

With the known shape of the source function, one can calculate theoretical diffusion curves for different parameters α and the calculated curves may be normalized for a certain position \vec{r}_N . The comparison of the experimental diffusion distributions, normalized in the same manner, and theoretical diffusion distributions, yields the experimental value for the parameter α . With this value and the known diffusion coefficient D , one can determine the effective depopulation rate R_m of the particular metastable state. More details about this method can be found in [9].

In the case of cylindrical symmetry, the following expression is derived by integration of the diffusion Eq. (7) over the observation axis z :

$$\left[\frac{\partial^2}{\partial \rho^2} + \frac{1}{\rho} \frac{\partial}{\partial \rho} \right] \int_z N_m(\vec{r}) dz + \left(\frac{\partial N(\vec{r})}{\partial z} \right)_{-\infty} - \left(\frac{\partial N(\vec{r})}{\partial z} \right)_{+\infty} - \alpha \int_z N_m(\vec{r}) dz = \bar{S}_m(\vec{r}), \quad (9)$$

where the radially dependent averaged source function is given by:

$$\bar{S}_m(\rho) = \int_z [S_1(\vec{r}) + S_2(\vec{r})] dz/D. \quad (10)$$

Generally, the solutions of a diffusion equation can be expressed as a series of modified Bessel functions which decrease exponentially for distances large in comparison with the size of the source region. Consequently, the asymptotic value for the derivative $\partial N_m(\vec{r})/\partial z$ in this limit is equal

to zero, and the Laplace operator in Eq. (9) reduces this to the one-dimensional form. Then, with the fulfilled condition $K_1(\rho) \propto \int N_1(\vec{r}) dz$, and taking into account the identity $N_m(\vec{r}) = N_1(\vec{r})(1 + M_{12}/M_{21})$, which is valid for the completely mixed metastable system, one obtains a modification of Eq. (7):

$$\left[\frac{\partial^2}{\partial \rho^2} + \frac{1}{\rho} \frac{\partial}{\partial \rho} \right] K_1(\rho) + \alpha K_1(\rho) = \bar{S}_m(\rho)/(1 + M_{12}/M_{21}). \quad (11)$$

The presented approach simplifies the problem at hand significantly and offers the opportunity to obtain data for the collisional deactivation of the lead metastables in an atmosphere outside the discharge zone.

5. Data analysis and results

Theoretical distributions $K(\rho)$ obeying Eq. (11) were calculated for parameter α in the range between 1 and 128 cm^{-2} . The averaged radially dependent source function $\bar{S}_m(\rho)$ was used in a form of a Gauss function, with the full width at half maximum $2\rho_0 = 1$ mm. This approximation fairly describes the experimental shape of the source zone (see Figs. 6 and 8). Theoretical diffusion curves were calculated applying the boundary condition $N_m(R_0) = 0$, where $R_0 = 15$ mm is the inner radius of the hot-pipe. In this way, the effect of destruction of the metastable atoms at the oven walls was included in the calculation. The present situation is very similar to that described in the paper of Vadla et al. [9] dealing with the diffusion of barium metastables. In the Ba work, the metastables were populated by the subsequent depopulation of a higher-lying level, which was directly excited by a laser from the ground state. The corresponding source function was well-defined rectangle of the similar size as in present case, whereas the boundary conditions were identical.

Using the axial electrode configuration [Fig. 1, inset (a)], the experimental distributions at various argon pressures were measured for distances

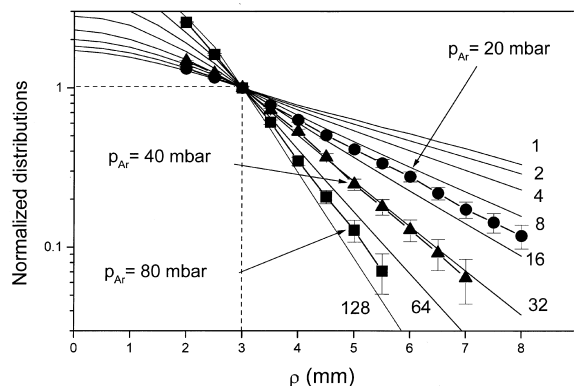


Fig. 10. Typical experimental diffusion distributions plotted in the field of theoretical distributions. The experimental distributions were obtained in the low discharge current mode and with axial electrode configuration. The numbers attributed to the theoretical curves are related to the parameter α expressed in units of cm^{-2} . See text for further explanations.

$\rho \geq 2$ mm. The theoretical, as well as the experimental, curves were normalized to unity at $\rho_N = 3$ mm, and typical results are plotted in Fig. 10. By fitting the experimental distributions into the field of theoretical curves, the experimental values for parameter α at various argon pressures were obtained. With these data, the values for the depopulation rates $R_m = D\alpha$ were calculated. The calculated values for R_m are plotted against the argon number density in Fig. 11.

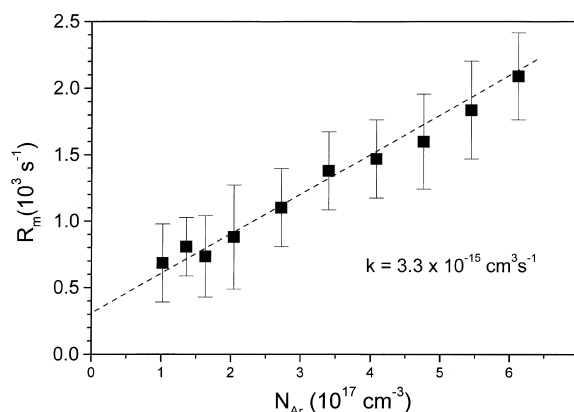


Fig. 11. Depopulation rate R_m of the metastable $\text{Pb } 6p^2 \text{ } ^3P_1$ complex in dependence on argon number density. The slope k of the straight-line fitted through the data set yields the value for the quenching rate coefficient.

The slope of the straight-line fitted through the data yields the rate $k_m = 3.3 \times 10^{-15} \text{ cm}^3 \text{ s}^{-1}$ for the quenching due to argon. The estimated total uncertainty of this value is approximately 20%. The calculated equilibrium density ratio N_2/N_1 at the experimental temperature amounts to 0.04. According to Eq. (8), the measured depopulation rate should be mainly attributed to the depopulation of the lower metastable state.

The straight-line intercepts the ordinate at the value of $\approx 300 \text{ s}^{-1}$. This residual rate comprises radiative relaxation rate A and a contribution R_{pb} due to quenching by ground-state lead atoms. Recently, in a separate absorption experiment [10], we have determined the transition probability A of the strictly forbidden ground to metastable state transition ${}^3\text{P}_0\text{--}{}^3\text{P}_1$, and found $A = 6.1 \text{ s}^{-1}$. This experimental value is in a good agreement with the latest theoretical result $A = 7.2 \text{ s}^{-1}$, which has been reported in [6]. Thus, the residual rate should be almost entirely ascribed to the ${}^3\text{P}_1$ state quenching by the ground-state lead atoms. Using the value $R_{\text{pb}} \approx 300 \text{ s}^{-1}$ and the actual ground-state density $N_0 = 5 \times 10^{14} \text{ cm}^{-3}$, we obtain quenching rate constant $k_{\text{pb}} \approx 6 \times 10^{-13} \text{ cm}^3 \text{ s}^{-1}$ for collisions with lead atoms. The error bar for this value is approximately 80%.

The latest data on the ${}^3\text{P}_1$ state quenching by argon and lead atoms can be found in [11]. The measurements of the Ar quenching rate were performed by varying Ar pressure in the range 100–700 torr, at constant lead density of $4 \times 10^{15} \text{ cm}^{-3}$ and temperature $T = 1193 \text{ K}$. From the rate vs. Ar pressure straight line, the authors obtained the quenching rate constant $k_{\text{Ar}} = 5.6 \times 10^{-16} \text{ cm}^3 \text{ s}^{-1}$, which is approximately seven times smaller than our present value. On the other hand, by extrapolating their measured data to zero argon pressure, the residual rate of $\approx 4 \times 10^3 \text{ s}^{-1}$ can be estimated. In addition, Reiser et al. [11] reported the value $k_{\text{pb}} = 2 \times 10^{-13} \text{ cm}^3 \text{ s}^{-1}$, which was obtained from the measurements performed by varying the Pb ground-state density. Taking into account either this value for k_{pb} or the value estimated in the present work, one can conclude that the residual rate of $\approx 4 \times 10^3 \text{ s}^{-1}$ in [11] should be mainly attributed to the radiative relax-

ation rate, which strongly disagrees with the recent theoretical and experimental results [6,10].

6. Conclusion

The production and loss processes of $6p^2 \text{ }^3\text{P}_1$ and $6p^2 \text{ }^3\text{P}_2$ lead metastable atoms in a low pressure argon discharge have been investigated. Under the present experimental conditions, the main losses of metastable populations are due to quenching by buffer gas atoms and the diffusion out of the zone where the metastables are created. Regarding the pressure dependence, the mentioned processes compete with each other in the opposite sense. Maximum population densities of the metastables, approximately 30% of the ground state density, were obtained at 40 mbar argon pressure and the highest current for stable discharge operation (30 mA). In addition, ${}^3\text{P}_1$ state quenching rate constants of $3.3 \times 10^{-15} \text{ cm}^3 \text{ s}^{-1}$ and $6 \times 10^{-12} \text{ cm}^3 \text{ s}^{-1}$ for collisions with argon and the ground-state Pb atoms, respectively, were determined.

Acknowledgements

The authors acknowledge gratefully financial support from the Deutsche Forschungsgemeinschaft within project no. 436 KRO 113/2/0 and the Ministry of Science and Technology of Republic of Croatia.

References

- [1] H.-D. Wizemann, K. Niemax, Cancellation of matrix effects and calibration by isotope dilution in isotope-selective diode laser atomic absorption spectrometry, *Anal. Chem.* 69 (1997) 4291–4293.
- [2] J. Franzke, H.-D. Wizemann, K. Niemax, C. Vadla, Impact broadening and shift rates for the $6p^2 \text{ }^3\text{P}_1^0 \rightarrow 7s \text{ }^3\text{P}_1^0$ transitions of lead induced by collisions with argon and helium, *Eur. Phys. J. D* 8 (2000) 23–28.
- [3] A.N. Nesmeyanov, *Vapor Pressure of Elements*, Academic Press, New York, 1963.
- [4] N.P. Penkin, I. Yu. Yu. Slavenas, Sil'i oscil'atorov spektral'nykh linyi SnI i PbI, *Opt. Spektrosk.* 15 (1963) 154–165 ([*Opt. Spectrosc. (USSR)* 15 (1963) 83]).

- [5] J. Franzke, D. Veza, M.A. Bratescu, K. Niemax, Pseudo-sonic wave detection in laser spectrometry, *Spectrochim. Acta Part B* 53 (1998) 613–620.
- [6] P. Horodecki, J. Kwela, J.E. Sienkiewicz, Transition probabilities of forbidden lines in Pb I, *Eur. Phys. J. D* 6 (1999) 435–440.
- [7] O. Axner, P. Ljungberg, Y. Malmsten, Lifetime measurements of metastable states of Au, Au, Bi, Cd, Mg, Pb, and Sr in an acetylene/air flame by laser-enhanced ionization spectroscopy, *Appl. Phys. B* 54 (1992) 144–155.
- [8] T.P. Redko, I. Kosinar, Diffusion coefficients of metals in inert gases: comparison of calculations with experimental data, *Czech. J. Phys. B* 30 (1980) 1293–1306.
- [9] C. Vadla, K. Niemax, V. Horvatic, R. Beuc, Population and deactivation of lowest lying barium levels by collisions with He, Ar, Xe and Ba ground state atoms, *Z. Phys. D* 34 (1995) 171–184.
- [10] C. Vadla, V. Horvatic, K. Niemax, Oscillator strength, isotope shift and hyperfine splitting of the strongly ‘forbidden’ Pb $6p^2\ ^3P_0 \rightarrow 6p^2\ ^3P_1$ transition at 1278.9 nm, *J. Phys. B* (submitted).
- [11] C. Reiser, N. Djeu, R. Burnham, Collisional quenching of Pb $6p^2\ ^3P_1$ and $6p^2\ ^3P_2$ metastables by ground state Pb atoms, *J. Chem. Phys.* 76 (1982) 2332–2337.